Journal of Statistical Physics, Vol. 107, Nos. 1/2, April 2002 (© 2002)

A Discrete Effect of the Thermal Lattice BGK Model

Michihisa Tsutahara[1] and Ho Keun Kang[1]

Received February 14, 2001; accepted November 27, 2001

In this article, a discrete effect in the thermal Lattice BGK two-speed model is studied. These effects are due to the non-equilibrium state in the particle distribution function, and the non-equilibrium occurs near walls. The mechanism of the LBM counterpart of the thermal creep flow, which appears due to the temperature gradient of the boundary in rarefied gases, is clarified analytically and numerical calculations are performed for some cases. A technique for eliminating this effect is also shown.

KEY WORDS: Lattice Boltzmann method; thermal BGK model; rarefied gas effect; thermal creep flow.

1. INTRODUCTION

In recent years, interest in the lattice Boltzmann method (LBM) has been rapidly increasing, and the number of applications has also been increasing from conventional ordinary fluids to complex fluids.[1–4]

The lattice Boltzmann method (LBM) is a method for simulating the motions of continuous fluids by computing the collision and the propagation of microscopic particles. This method has been developed from the lattice gas automata (LGA),[5–7] but recently the lattice Boltzmann equation has been rigorously derived from the ordinary Boltzmann equation in kinetic theory.[8–10] Therefore, the lattice Boltzmann equation can be understood to have a sound connection with fluid dynamics. Essentially, this method is considered to simulate the Navier–Stokes equations, and actually, the Navier–Stokes equations are derived by the so-called Chapman–Enskog expansion technique. But the particles translate from one lattice

[1] Graduate School of Science and Technology, Kobe University, Rokko, Nada-ku, Kobe 657-8501, Japan; e-mail: tutahara@mech.kobe-u.ac.jp

0022-4715/02/0400-0479/0 © 2002 Plenum Publishing Corporation

site to a neighboring site without collision, and the lattice size can be considered to be the counter part of the order of the mean free path in molecular gas dynamics. The lattice size is not necessarily small when compared with the length scale.

In molecular gas dynamics, when the Knudsen number (ratio of the mean free path to the length scale) is not very small, various rarefied gas effects appear, and the flow field becomes different from those obtained by the Navier–Stokes equations.

In the LBM, the counter part of the Knudsen number (ratio of the lattice size to the length scale) is not small, so some similar effect should appear. This effect is unphysical but it is due to the finite size of the lattice. Therefore, this effect is called the "discrete effect." The same kind of effect has been investigated in connection with the slip on the solid boundary for the LGA[11, 12] and for the LBM.[13, 14]

In this study, the LBM counterpart of the thermal creep flow, which appears due to the temperature gradient of the boundary in rarefied gases,[15] is studied. The two-speed model is used and it is shown that the steady flow is induced in the direction of the temperature gradient parallel to the boundary surface.

By a simple analysis, it is clarified that this flow is driven by the particles emitting from the boundary and some numerical examples are also presented.

2. THE THERMAL LATTICE BGK MODEL

There are two kinds of models in the lattice Boltzmann method; one is a non-thermal model and the other is a thermal model. The energy conservation of the particles is not considered in the non-thermal models, even though they have compressible features. On the other hand, thermal models include energy conservation at the particle collision,[2, 16] and they can treat compressible fluids rigorously. In the thermal models, multi-speed particles, in general, are necessary in order to increase the degree of the particle energy.

2.1. The Lattice BGK Equation

The lattice Boltzmann model employed here uses a hexagonal grid in which each site is connected to its six nearest neighbors as shown in Fig. 1. The particles translate along lattice lines of sizes Δ with constant speeds, which allow moving particles to reach the neighboring lattice sites during one time step. After translation, the particles collide with each other on

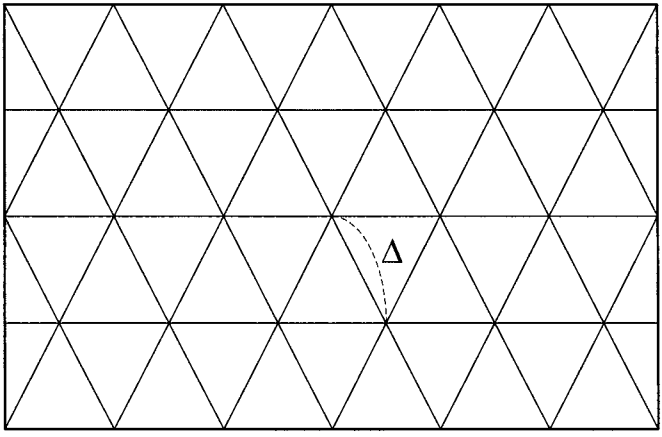

Fig. 1. Hexagonal lattice.

lattice sites according to the rule to conserve the mass, momentum, and energy.

The lattice BGK model employs the single time relaxation parameter which Bhatnagar, Gross and Krook[17] first introduced in order to simplify the collision term in the Boltzmann Eq. (18). For this study, the two-speed model (D2Q13) as shown in Fig. 2 was used because this model is simplest in the two-dimensional thermal BGK model. For other models, the same discussion can be directly applied and the same result will be obtained.

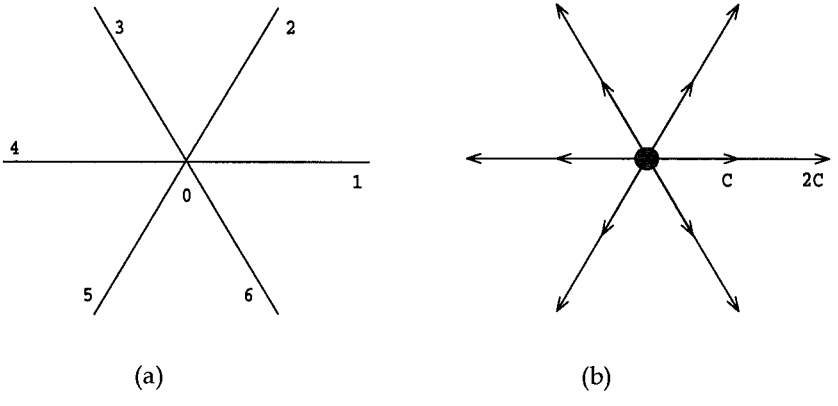

Fig. 2. Particle traveling directions and 2D13V model.

Let the distribution function be denoted as $f_{\sigma,i}$, where subscript σ represents the particle speed and $\sigma = 0, 1, 2$ for this model, and i represents the direction of translation and $i = 1, 2, ..., 6$ if $\sigma \neq 0$. The distribution function of particles with velocity $\mathbf{c}_{\sigma i}$ at site $\mathbf{r}$ at time t is evolved according to the lattice BGK equation,

$$f_{\sigma,i}(t+\tau, \mathbf{r}+\mathbf{c}_{\sigma,i}\tau) = f_{\sigma,i}(t, \mathbf{r}) - \frac{1}{\phi}\left(f_{\sigma,i}(t, \mathbf{r}) - f^{(0)}_{\sigma,i}(t, \mathbf{r})\right) \tag{1}$$

where $\mathbf{c}_{\sigma i,}$ is the velocity vector in the i-th direction with $|\mathbf{c}_{\sigma,i}| = \sigma c$ and $f^{(0)}_{\sigma,i}(t, \mathbf{r})$ is the local equilibrium distribution function. The second term on the right hand side of (1) is the collision operator, and ϕ is the relaxation time coefficient. This collision operator shows the particle distribution function approaches an equilibrium state during the collision step.

The dynamics of the fluid can be described by the distribution function obeying the lattice BGK Eq. (1). Here, the fundamental physical variables are the density ρ, the fluid momentum ρu_α and the total energy of the fluid $\frac{1}{2}\rho u^2 + \rho e$, which are related to the distribution function by,

$$\rho = \sum_{\sigma,i} f_{\sigma,i} = \sum_{\sigma,i} f^{(0)}_{\sigma,i} \tag{2}$$

$$\rho u_\alpha = \sum_{\substack{\sigma,i \\ \sigma,i}} f\, \mathbf{c}_{\sigma,i,\alpha} = \sum^{(0)}_{\substack{\sigma,i \\ \sigma,i}} f\, \mathbf{c}_{\sigma,i,\alpha} \tag{3}$$

$$\tfrac{1}{2}\rho u^2 + \rho e = \sum_{\sigma,i} \tfrac{1}{2} f_{\sigma,i} c^2_{\sigma,i,\alpha} = \sum_{\sigma,i} \tfrac{1}{2} f^{(0)}_{\sigma,i} c^2_{\sigma,i,\alpha} \tag{4}$$

where u_α is the component of flow velocity, and e is the internal energy of the fluid per unit volume. The index α represents the Cartesian component.

2.2. Macroscopic Governing Equations of Fluid

The continuum hydrodynamic equations modeled by this dynamic scheme can be determined by performing a Chapman–Enskog expansion on the lattice BGK equation (1). Equation (1) can be Taylor expanded to the second order as

$$\frac{\partial f_a}{\partial t} + c_{a\alpha}\frac{\partial f_a}{\partial r_\alpha} + \frac{1}{2}\tau c_{a\alpha} c_{a\beta}\frac{\partial^2 f_a}{\partial r_\alpha\, \partial r_\beta} + \tau c_{a\alpha}\frac{\partial^2 f_a}{\partial t\, \partial r_\alpha} + \frac{1}{2}\tau\frac{\partial^2 f_a}{\partial t^2} \cong -\frac{1}{\tau\phi}\left(f_a - f^{(0)}_a\right) \tag{5}$$

where subscript a represents σ, i in (1) for simplicity, and α and β represent the Cartesian components. By expanding the distribution function and the time and space derivatives as,

$$\begin{aligned} f_a &= f_a^{(0)} + f_a^{neq} = f_a^{(0)} + \varepsilon f_a^{(1)} + \varepsilon^2 f_a^{(2)} + \cdots, \\ \frac{\partial}{\partial t} &\to \varepsilon \frac{\partial}{\partial t_1} + \varepsilon^2 \frac{\partial}{\partial t_2}, \\ \frac{\partial}{\partial r_\alpha} &\to \varepsilon \frac{\partial}{\partial r_{1\alpha}} \end{aligned} \tag{6}$$

and using (5), the Chapman–Enskog expansion can be performed. Substituting (6) into (5) and collecting terms up to $O(\varepsilon^2)$ obtains

$$\left(\frac{\partial}{\partial t_1} + \frac{\partial}{\partial t_2}\right) f_a^{(0)} + c_{a\alpha} \frac{\partial f_a^{(0)}}{\partial r_{1\alpha}} + \left(1 - \frac{1}{2\phi}\right)\left[\frac{\partial f_a^{(1)}}{\partial t_1} + c_{a\alpha} \frac{\partial f_a^{(1)}}{\partial r_{1\alpha}}\right] = -\frac{1}{\tau\phi}\left(f_a^{(1)} + f_a^{(2)}\right) \tag{7}$$

This must lead to the continuity equation,

$$\frac{\partial \rho}{\partial t} + \frac{\partial}{\partial r_{1\alpha}}(\rho u_\alpha) = 0 \tag{8}$$

the Navier–Stokes equations,

$$\frac{\partial}{\partial t} \rho u_\alpha + \frac{\partial}{\partial r_{1\beta}}(\rho u_\alpha u_\beta) = -\frac{\partial P}{\partial r_{1\alpha}} + \frac{\partial}{\partial r_{1\beta}} \mu \left(\frac{\partial u_\beta}{\partial r_{1\alpha}} + \frac{\partial u_\alpha}{\partial r_{1\beta}}\right) + \frac{\partial}{\partial r_{1\alpha}}\left(\lambda \frac{\partial u_\gamma}{\partial r_{1\alpha}}\right) \tag{9}$$

and the energy equation for the macroscopic fluid,

$$\begin{aligned} &\frac{\partial}{\partial t}\left(\rho e + \frac{1}{2}\rho u^2\right) + \frac{\partial}{\partial r_{1\alpha}}\left(\rho e + P + \frac{1}{2}\rho u^2\right) u_\alpha \\ &\quad = \frac{\partial}{\partial r_{1\alpha}}\left(k \frac{\partial e}{\partial r_{1\alpha}}\right) + \frac{\partial}{\partial r_{1\alpha}}\left\{\mu u_\beta \left(\frac{\partial u_\beta}{\partial r_{1\alpha}} + \frac{\partial u_\alpha}{\partial r_{1\beta}}\right)\right\} + \frac{\partial}{\partial r_{1\alpha}}\left(\lambda \frac{\partial u_\beta}{\partial r_{1\beta}} u_\alpha\right) \end{aligned} \tag{10}$$

The pressure P, the viscosity μ, the second viscosity λ and the conductivity of the internal energy κ of this fluid are given, respectively by,

$$\begin{aligned} &P = \frac{2}{D}\rho e, \qquad \mu = \frac{2}{D}\rho e \tau\left(\phi - \frac{1}{2}\right), \qquad \lambda = -\frac{4}{D^2}\rho e \tau\left(\phi - \frac{1}{2}\right), \\ &\kappa = \frac{2(D+2)}{D^2}\rho e \tau\left(\phi - \frac{1}{2}\right) \end{aligned} \tag{11a,b,c,d}$$

where D indicates the dimension and 2 in this case.

2.3. The Equilibrium Distribution Function

The local equilibrium distribution function is expressed as,

$$f_{\sigma i}^{(0)} = F_\sigma \rho \left[1 - 2Bc_{\sigma i\alpha}u_\alpha + 2B^2 c_{\sigma i\alpha}c_{\sigma i\beta}u_\alpha u_\beta + Bu^2\right] \tag{12}$$

The moving particles are allowed to move with two kinds of speed, c, $2c$. The unknown factors in (12), that is F_0, F_1, F_2, and B are determined according to the constraints that (12) satisfies (2), (3), and (4), and that the macroscopic equation governing the fluid motion corresponds to the Navier–Stokes equations. The functions, F_0, F_1, F_2, are determined as,

$$F_0 = 1 + \frac{1}{4B^2c^4}(2 + 5Bc^2), \qquad F_1 = -\frac{1}{9B^2c^4}(1 + 2Bc^2),$$

$$F_2 = \frac{1}{36B^2c^4}\left(1 + \frac{1}{2}Bc^2\right) \tag{13a,b,c}$$

and,

$$B = -\frac{1}{2e} \tag{14}$$

3. THERMAL CREEP FLOW IN THE THERMAL LATTICE BGK MODEL

For rarefied gases, extended studies[15] on the thermal creep flow have been performed so far. In the continuous limit, this flow can be negligible. However, in the thermal LBM model, this false flow can be significant even when considering that this model is a solver of the Navier–Stokes equation. This is shown by the following simple analysis.

3.1. The Case Without a Wall

Consider a two-dimensional flow being at rest with a linear internal energy or temperature gradient in the x-direction. First, the x-direction is taken in the direction perpendicular to the lattice line as shown in Fig. 3. The an-isotropic feature of the lattice shall be considered later. No body force is taken into account. The pressure is represented by $P = \rho e$ and is assumed to be constant, say P_0. As the pressure is uniform, the density gradient is inverse to that of the internal energy. The increment of the internal energy between neighboring sites is denoted by $\frac{de}{dx}\frac{\sqrt{3}}{2}\Delta$, where Δ denotes lattice size, i.e., the distance between the neighboring sites, and the

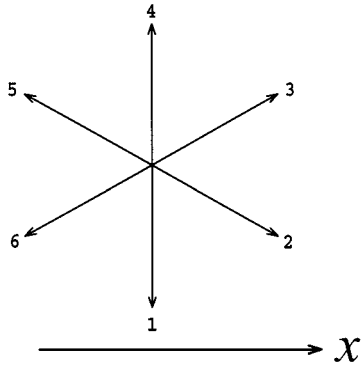

Fig. 3. Lattice line and the x direction (1).

internal energy gradient is assumed as being constant. Then the density distribution is expressed as, $\rho = P_0/e$.

For simplicity, any change in the direction perpendicular to the x-direction (see Fig. 3) is not considered, that is one dimensional flow in the flow domain, and the local equilibrium distribution functions are considered at points on five neighboring columns as shown in Fig. 4. The internal energy and the density do not change along each column. Then, the local equilibrium functions for zero velocity are,

$$f_{1,i}^{(0)}(\pm 1) = -\frac{4P_0}{9}\left(e \pm \frac{de}{dx}\frac{\sqrt{3}}{2}\Delta - 1\right),$$
$$f_{2,i}^{(0)}(\pm 2) = \frac{P_0}{9}\left(e \pm 2\frac{de}{dx}\frac{\sqrt{3}}{2}\Delta - \frac{1}{4}\right), \qquad (i = 1, 2, \ldots, 6) \tag{15}$$

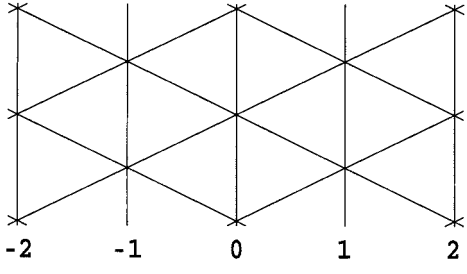

Fig. 4. Definition of neighboring sites.

where $c=1$ is put in (13) and the time increment $\tau=\Delta/c=\Delta$ is taken hereafter without any loss of generality. Here only the following two steps are considered; that is the translation and the collision stages of the particles. The distribution function after the translation (after the time increment τ) at the site "0" will be,

$$f_{1,3}(0)=-\frac{4P_0}{9}\left(e-\frac{de}{dx}\frac{\sqrt{3}}{2}\Delta-1\right),\quad f_{1,5}(0)=-\frac{4P_0}{9}\left(e+\frac{de}{dx}\frac{\sqrt{3}}{2}\Delta-1\right),$$
$$f_{2,3}(0)=\frac{P_0}{9}\left(e-2\frac{de}{dx}\frac{\sqrt{3}}{2}\Delta-\frac{1}{4}\right),\quad f_{2,5}(0)=\frac{P_0}{9}\left(e+2\frac{de}{dx}\frac{\sqrt{3}}{2}\Delta-\frac{1}{4}\right) \tag{16}$$

and f_0 does not change. No consideration to $f_{\sigma,1}$ or $f_{\sigma,4}$ is given here, because they have nothing to do with the velocity in the x-direction. The assumption of the flow velocity being 0 in the direction perpendicular to the x-direction results in,

$$f_{1,3}=f_{1,2},\qquad f_{2,3}=f_{2,2},\qquad f_{1,5}=f_{1,6},\qquad f_{2,5}=f_{2,6} \tag{17}$$

Then the flow velocity in the x-direction at this point is,

$$u=\frac{2}{\rho}\left[f_0\times 0+f_{1,1}\times\sqrt{3}+f_{1,2}\times(-\sqrt{3})+f_{2,1}\times 2\sqrt{3}+f_{2,2}\times(-2\sqrt{3})\right]=0 \tag{18}$$

and as is evident, there is naturally no flow.

After the collision stage, there is no flow also because at the collision the momentum is conserved at each lattice site regardless of the value of the relaxation time coefficient ϕ.

When there is no boundary, the distribution functions in a steady state at a lattice site, say, site "0" are,

$$\begin{aligned}
f_{s1,3}(0)&=-\frac{4P_0}{9}\left(e+(1-\phi)\frac{de}{dx}\frac{\sqrt{3}}{2}\Delta-1\right),\\
f_{s1,5}(0)&=-\frac{4P_0}{9}\left(e-(1-\phi)\frac{de}{dx}\frac{\sqrt{3}}{2}\Delta-1\right),\\
f_{s2,3}(0)&=\frac{P_0}{9}\left(e+2(1-\phi)\frac{de}{dx}\frac{\sqrt{3}}{2}\Delta-\frac{1}{4}\right),\\
f_{s2,5}(0)&=\frac{P_0}{9}\left(e-2(1-\phi)\frac{de}{dx}\frac{\sqrt{3}}{2}\Delta-\frac{1}{4}\right)
\end{aligned} \tag{19}$$

where the distribution function for the rest particles is not considered because it does not matter in this analysis. As in (17), there is also,

$$f_{s1,3} = f_{s1,2}, \quad f_{s2,3} = f_{s2,2}, \quad f_{s1,5} = f_{s1,6}, \quad f_{s2,5} = f_{s2,6} \tag{20}$$

These functions induce no velocity, but the thermal energy flux does exist.

3.2. The Effect of Wall

Consider the situation where wall extending in the x-direction with the same temperature gradient as that in the flow domain is inserted in the fluid in a steady state as shown in Fig. 5. At the surface, the diffusive reflection of the particles, that is the particles reflecting in the manner of the local equilibrium distribution or Maxwellian distribution, is assumed. The equilibrium distribution function at the surface is determined by (12), (13) and (14) using the temperature or the internal energy at the surface and zero velocity and the density calculated from incoming and outgoing particles. Then the distribution functions are uniquely determined and symmetric with respect to the plane perpendicular to the x-direction. The particles in directions 3 and 5 on the wall surface as shown in Fig. 5 where the no-slip local equilibrium distribution function is applied are given as,

$$f_{w1,3}(-1) = -\frac{4P_0}{9}\left(e - \frac{de}{dx}\frac{\sqrt{3}}{2}\Delta - 1\right), \quad f_{w1,5}(1) = -\frac{4P_0}{9}\left(e + \frac{de}{dx}\frac{\sqrt{3}}{2}\Delta - 1\right),$$
$$f_{w2,3}(-1) = \frac{P_0}{9}\left(e - \frac{de}{dx}\frac{\sqrt{3}}{2}\Delta - \frac{1}{4}\right), \qquad f_{w2,5}(1) = \frac{P_0}{9}\left(e + \frac{de}{dx}\frac{\sqrt{3}}{2}\Delta - \frac{1}{4}\right) \tag{21}$$

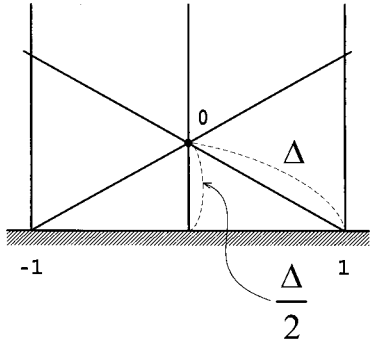

Fig. 5. Wall and lattice (1).

The particles of speed $c\,(=1)$ move to the site "0" after the translation in time increment τ, and the particles of speed $2c\,(=2)$ move to the same point after $\tau/2$. Therefore the particles in directions 3 and 5 at the site "0" are obtained by replacing 1 and -1 with 0 in the first two expressions in (21). The particles in directions 2 and 6 are given by (19) and (20), and

$$\begin{aligned}
f_{1,3}(0) &= -\frac{4P_0}{9}\left(e+(1-\phi)\frac{de}{dx}\frac{\sqrt{3}}{2}\Delta-1\right),\\
f_{1,5}(0) &= -\frac{4P_0}{9}\left(e-(1-\phi)\frac{de}{dx}\frac{\sqrt{3}}{2}\Delta-1\right),\\
f_{2,3}(0) &= \frac{P_0}{9}\left(e+2(1-\phi)\frac{de}{dx}\frac{\sqrt{3}}{2}\Delta-\frac{1}{4}\right),\\
f_{2,5}(0) &= \frac{P_0}{9}\left(e-2(1-\phi)\frac{de}{dx}\frac{\sqrt{3}}{2}\Delta-\frac{1}{4}\right)
\end{aligned} \tag{22}$$

Then, the velocity is,

$$\begin{aligned}
u &= \frac{1}{\rho}\Bigg[f_0\times 0+f_{w1,3}\times\frac{\sqrt{3}}{2}+f_{w1,5}\times\left(-\frac{\sqrt{3}}{2}\right)+f_{w2,3}\times\sqrt{3}+f_{w2,5}\times\left(-\sqrt{3}\right)\\
&\quad +f_{w1,2}\times\frac{\sqrt{3}}{2}+f_{w1,6}\times\left(-\frac{\sqrt{3}}{2}\right)+f_{w2,2}\times\sqrt{3}+f_{w2,6}\times(-\sqrt{3})\Bigg]\\
&= \frac{4P_0}{9\rho}\frac{de}{dx}\frac{\sqrt{3}}{2}\Delta
\end{aligned} \tag{23}$$

or

$$u = \frac{4}{9}e\frac{de}{dx}\frac{\sqrt{3}}{2}\Delta = \frac{2}{9}\frac{d(e)^2}{dx}\frac{\sqrt{3}}{2}\Delta \tag{24}$$

Equation (23) shows that the flow is induced in the direction of the temperature gradient; that is, the parallel direction in the vicinity of the wall. It should be noted here that this flow is induced by the imbalance of the particles from the wall given by (21) and the particle from the flow domain given by (22) does not induce any flow. Also of note is that this driving force acts on the lattice site at a distance of one lattice from the wall for the two-speed particle model. If a three-speed model is used, the driving force will reach a distance of two lattices. If the flow field extends to infinity from the wall, a steady flow will be obtained by the following consideration. In the vicinity of the wall, the fluid receives the momentum presented

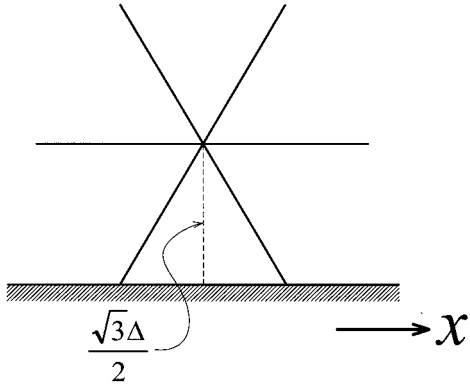

Fig. 6. Wall and lattice (2).

in (23), where the fluid has finite velocity or not. Therefore, if the fluid gives the same momentum to the wall, through the particles moving in the directions 2 and 6 in Fig. 6, then the flow will establish a steady state. If velocity at a point next to the wall is assumed to be completely parallel to the wall, then (20) would hold and this flow should have a momentum twice as large as that which the flow obtains from the wall. So, the flow velocity is estimated as,

$$u = \frac{8P_0}{9\rho}\frac{de}{dx}\frac{\sqrt{3}}{2}\Delta \tag{25}$$

This is the thermal creep flow of the lattice BGK model, and the velocity is proportional to the temperature gradient, the pressure and the lattice scale for given density. When $\Delta \to 0$, this flow disappears and may be referred to as the "continuous limit of FDLBM."

3.3. Lattice Dependence or An-Isotropic Feature

Consider the situation where the relation between the lattice and the wall is changed as in Fig. 6, where the wall is perpendicular to the one lattice line. In this case, the particles moving in all directions must be considered. The details have been omitted here but the driven velocity at the nearest point from the wall is obtained as,

$$u = \frac{4P_0}{9\rho}\frac{de}{dx}\frac{\sqrt{3}}{2}\Delta \tag{26}$$

This is the same as that in the previous case. It should be noted, however, that the point on which the driving force acts is a distance of $\frac{\sqrt{3}}{2}\Delta$ from the wall in this case, whereas it was $\frac{\Delta}{2}$ in the previous case. In other words, the driving force reaches more deeply inside the flow domain in the present case than in the previous case. This difference does not matter when the half-infinite domain is considered, but the difference is significant for the finite domain. Therefore, this flow, a counterpart of the thermal creep flow, is not isotropic in nature.

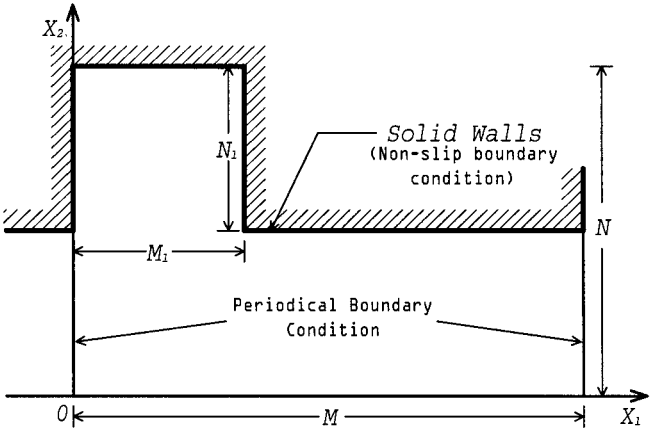

(a)

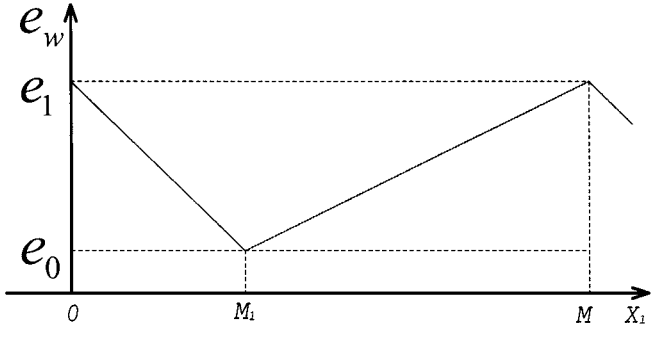

(b)

Fig. 7. A sketch of the one-way flow channel: (a) Channel shape (one section) and (b) temperature distribution.

4. NUMERICAL EXAMPLES

4.1. One-Way Flow in a Channel

Here, a striking result of the rarefied effect of the thermal lattice BGK model is displayed. Consider a two-dimensional channel with a square cavity. The lower side is the line of symmetry, so that mirror reflection is applied. Linear temperature (internal energy) gradients are fixed from the lowest internal energy e_0 to the highest internal energy e_1 on the wall as shown in Fig. 7(a) and (b), and the right and the left sides are the periodic boundaries. By this shape of channel, Sone *et al.*[18] show that for rarefied gases, one-way flow in the rightward direction exists. In molecular gas dynamics, this phenomenon is sometimes called the "thermal transpiration flow." In the lattice thermal BGK flow, which includes several speeds, a counterpart of the thermal transpiration flow appears.

The number of the lattice is $M \times N = 60 \times 40$, $M_1 = 20$ and $N_1 = 20$. The relaxation time coefficient ϕ is kept at 0.6, and the internal energy $e_0 = 0.5$ and $e_1 = 0.7$. The initial conditions are as follows: The fluid density is $\rho = 1.225$, and the internal energy $e = 0.5$ in the entire flow field.

Figure 8 shows the velocity field. A one-way rightward flow is induced in the channel, and there is a counter clockwise circulation flow in the cavity even without any body force. It is observed that the flow is induced in the direction of the temperature gradient in the vicinity of the wall.

Figure 9 shows the time history of the mean flow velocity over the cross-section at the right boundary. The velocity increases as the time increases but it reaches a steady state.

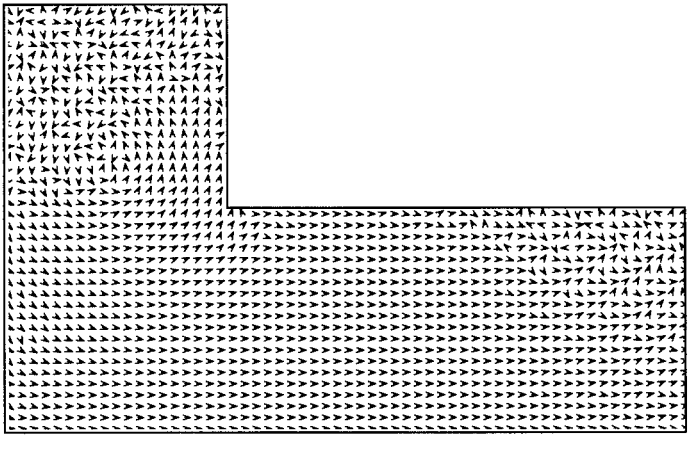

Fig. 8. Velocity vectors in the channel.

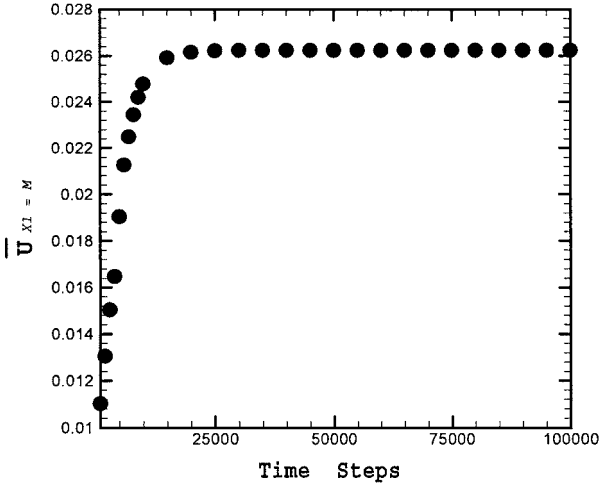

Fig. 9. The mean flow velocity in the x-direction over the cross section at the origin.

It should be noted here that this flow is unrealistic because the lattice Boltzmann model is, as stated above, a Navier–Stokes solver, and a technique for eliminating this effect must be employed. This technique shall be discussed later.

4.2. Two Dimensional Cavity with Temperature Gradients on the Both Sides

Consider a domain inside a square cavity with the temperature gradient on the sides as shown in Fig. 10. The lattice is set so that one of lattice lines

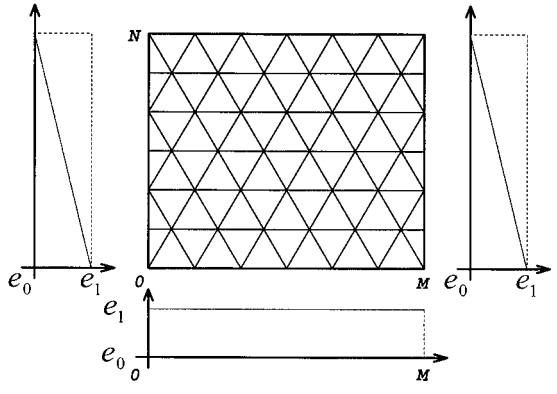

Fig. 10. Sketch of the cavity with thermal gradients on both sides.

is perpendicular to the sides. The internal energy on the top wall is $e_0 = 0.50$ and that on the bottom wall $e_1 = 0.70$, and the linear gradient is given on both sides. The number of the lattice is $M \times N = 60 \times 60$, the initial density $\rho = 1.225$ and the internal energy $e = 0.50$.

In this thermal BGK model, the heat conductivity in (11d) is nearly constant in a steady state because $p = \rho e$ is nearly constant. Therefore, the contours of constant internal energy (temperature) should be parallel to the top or bottom wall and there should not be any flow.

Figure 11 shows the velocity vectors, and downward flows can be observed on both sides in which two circulation flows are established. The calculated speed at the point on the horizontal centerline and nearest from the wall is 0.855×10^{-6} whereas 1.56×10^{-6} by the theory presented in (25). The difference is probably due to the appearance of strong shear in the calculation because of the counter flow, and this is clearly shown later in Fig. 16(a).

Because of this flow, the internal energy (temperature) distribution is different from that expected and is shown by circles in Fig. 12; that is, the contours of constant internal energy are not straight unlike the theoretical one.

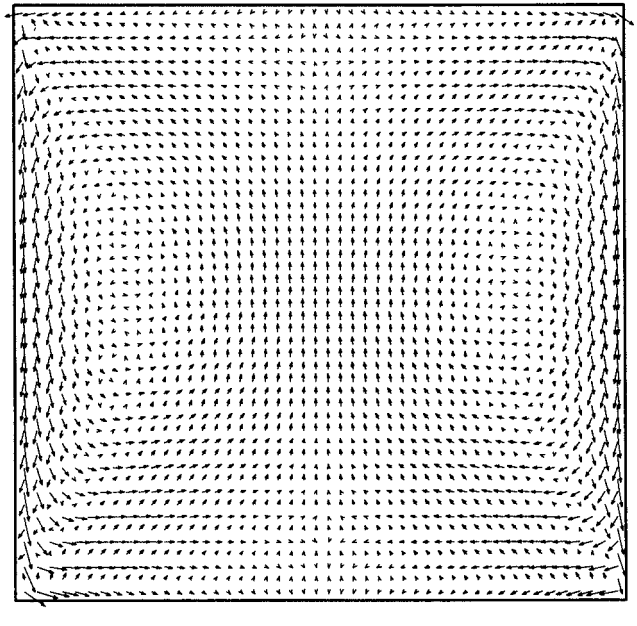

Fig. 11. Velocity vectors in the cavity.

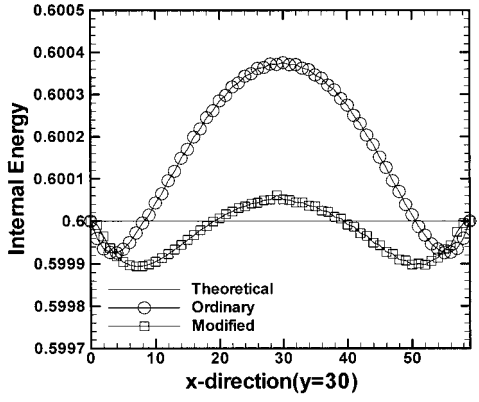

Fig. 12. The internal energy distribution along the horizontal centerline. ○: Ordinary boundary condition, □: Modified boundary condition presented in Section 5.

Figure 13 is the relationship between the internal energy (temperature) gradient and the flow velocity at the point on the horizontal centerline of the cavity and nearest to the right side. On this point, the density is almost constant even if the internal energy gradient is changed. The velocity increases in proportion to the temperature gradient, and it supports (25).

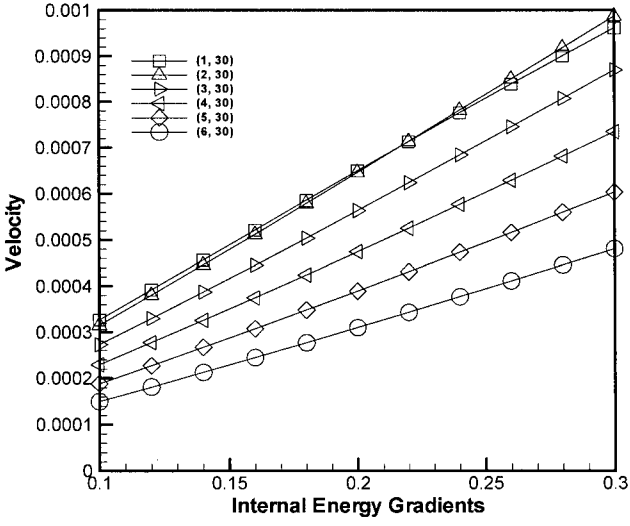

Fig. 13. The relationship between internal energy gradient and velocity.

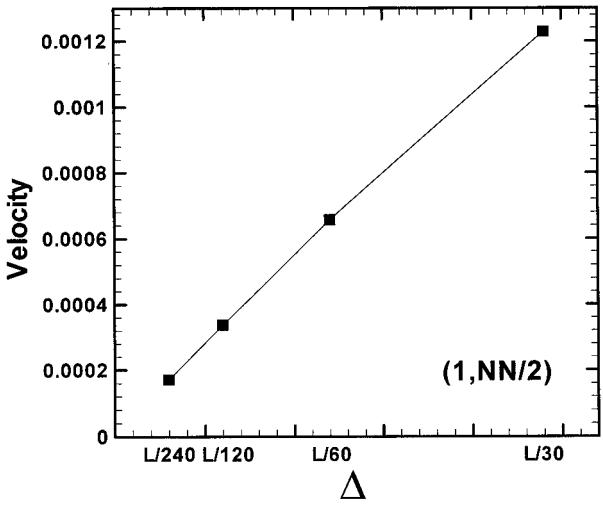

Fig. 14. The relationship between lattice size and velocity.

Figure 14 shows the relationship between the lattice size and the flow velocity. The lattice size is changed by changing the number of the lattice in the same domain. The value of L in this figure is $L = 2 \times$(The cavity height)$/\sqrt{3}$. The flow velocity increases linearly with the lattice size, and when $\Delta \to 0$, the flow is eliminated. This means that when the lattice is sufficiently fine, this unrealistic effect will be neglected, but when the lattice is coarse, the calculated results must be carefully checked.

4.3. An-Isotropic Nature of the Flow

The results of two cases are compared to check the independence of the flow on the lattice. One of the lattice lines is perpendicular to the side (Model 1), and the other parallel to the side (Model 2). The square cavity is considered by taking the number of the lattice as $M \times N = 52 \times 60$ in order to make the geometrical configuration the same. Figure 15 shows the velocity distribution in the vertical direction (parallel direction to the side) along the horizontal center-line. At the sites nearest the wall, the driving force should be the same, but the positions of the nearest sites are different for both cases, and then the velocity distributions are different from each other. In this sense, this flow is anisotropic in nature, which corresponds to the anisotropic nature of the Knudsen layer in LGA(11).

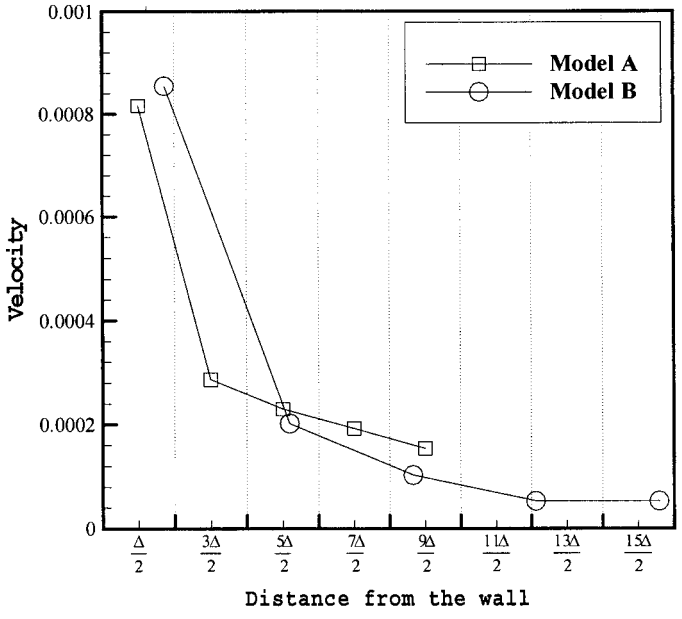

Fig. 15. Anisotropic feature of the flow.

5. DISCUSSION AND A TECHNIQUE TO ELIMINATE THE FLOW

As stated above, this discrete effect should be eliminated for simulating the fluid motion governed by the Navier–Stokes equations. The flow is induced by the imbalance of the particles coming from the wall given by (21). More precisely, for the two-speed model, if the particles of speed 2c coming from a site at a distance of two-lattices with the state there, nothing happens as shown in (18). But if they come from a site on the wall at a distance of one lattice, then the term $2\frac{de}{dx}\frac{\sqrt{3}}{2}\Delta$ in $f_{2,3}$ and $f_{2,5}$ in (16) is changed by $\frac{de}{dx}\frac{\sqrt{3}}{2}\Delta$ in (21), and this situation does occur. In order to eliminate this discrete effect, the site where estimation is made on the particles of speed 2c should be moved to a site at a distance of two lattices from the site "0." That is to say, the site is extended inside the wall and the temperature (internal energy) and the density are suitably assumed there.

The velocity distributions along the centerline are shown in Fig. 16, in which ordinary velocity is in (a) and that obtained by the above technique. In this technique, the internal energy is determined by the value on the side assuming it does not change in the horizontal direction, and the pressure is assumed as constant P_0; therefore, the density is determined so that

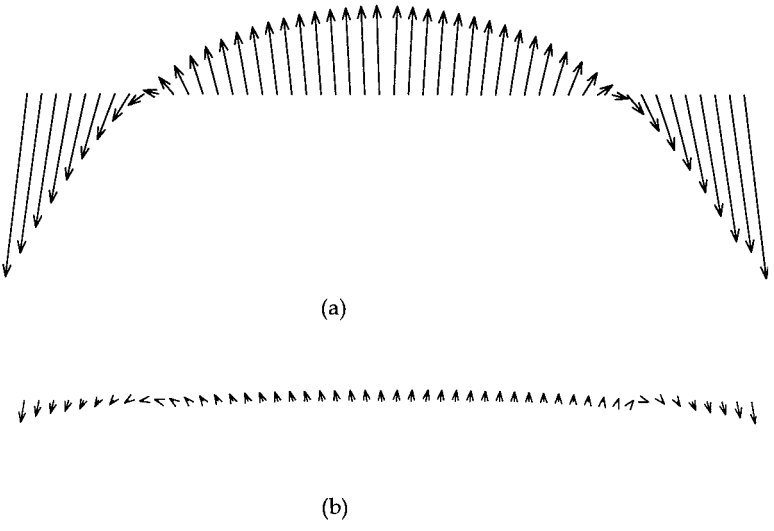

Fig. 16. Velocity distribution along the horizontal centerline: (a) Velocity by ordinary boundary condition, (b) velocity by modified boundary condition

$\rho = P_0/e$. In order words, the same functions as $f_{2,3}$ and $f_{2,5}$ in (16) are used instead of those in (21). The contours of constant internal energy $e = 0.6$ are shown by the square in Fig. 12, and it can be observed that the variation becomes much smaller and more horizontal.

6. CONCLUSIONS

A discrete effect in the thermal lattice BGK model, especially a counterpart of the thermal creep flow in rarefied gases, which is induced by the temperature gradient of walls, is clarified by simple analysis and numerical simulations. This flow is proportionate to the temperature gradient of the wall and the lattice size for cases of constant pressure and density. If some lattice sites are considered inside the wall, this unrealistic effect is shown to be considerably eliminated.

REFERENCES

1. F. J. Alexander, S. Chen, and J. D. Sterling, Lattice Boltzmann thermo-hydrodynamics, *Phys. Rev. E* **47**:2249–2252 (1993).
2. Y. Chen, H. Ohashi, and M. Akiyama, Thermal lattice Bhatnagar–Gross–Krook model without nonlinear deviations in macrodynamic equation, *Phys. Rev. E* **50**:2776–2783 (1994).

3. J. Huang, F. Xu, M. Vallieres, D. H. Feng, Y. H. Qian, B. Fryxell, and M. R. Strayer, A thermal LBGK model for large density and temperature differences, *Internat. J. Modern Phys. C* **8**(4):827–841 (1997).
4. N. Takada, A study of simulation of fluid motion by the lattice Boltzmann method, Doctor Dissertation (1998), in Japanese.
5. G. McNamara and G. Zanetti, Use of the Boltzmann equation to simulate lattice-gas automata, *Phys. Rev. Lett.* **61**:2332–2335 (1988).
6. Y. H. Qian, S. Succi, and S. A. Orszag, Recent advances in lattice Boltzmann computing, *Ann. Rev. of Comp. Phy. III*, D. Stauffer, ed. (World Scientific, 1995).
7. D. Rothman and S. Zaleski, *Lattice-Gas Cellular Automata* (Cambridge University Press, 1997).
8. X. He and L-S. Luo, Theory of the lattice Boltzmann method: From the Boltzmann equation to the lattice Boltzmann equation, *Phys. Rev. E* **56**(6):6811–6817 (1997).
9. X. He and L-S. Luo, A priori derivation of the lattice Boltzmann equation, *Phys. Rev. E* **55**(6):6333–6336 (1997).
10. T. Abe, Derivation of the lattice boltzmann method by means of the discrete ordinate method for the Boltzmann equation, *J. Comp. Phys.* **131**:241–246 (1997).
11. R. Cornubert, D. D'humieres, and D. Levermore, A Knudsen layer theory of lattice gases, *Physica D* **47**:241–259 (1991).
12. L-S. Luo *et al.*, Generalized hydrodynamic transport in lattice-gas automata, *Phys. Rev. A* **43**(12):7097–7100 (1991).
13. L-S. Luo, Analytic solution of linearized lattice Boltzmann equation for simple flows, *J. Stat. Phys.* **88**(3/4):913–925 (1997).
14. X. He *et al.*, Analytic solutions of simple flows and analysis of nonslip boundary conditions for the lattice Boltzmann BGK model, *J. Stat. Phys.* **87**(1/2):115–136 (1997).
15. Y. Sone, Flows induced by temperature fields in a rarefied gas and their ghost effect on the behavior of a gas in the continuum limit, *Ann. Rev. Fluid Mech.* **32**:779–811 (2000).
16. F. J. Alexander, S. Chen, and J. D. Stering, Lattice Boltzmann thermodynamics, *Phys. Rev. E* **47**(4):2249–2252 (1993).
17. P. L. Bhatnagar, E. P. Gross, and M. Krook, A model for collision processes in gases. I. Small amplitude processes in charged and neutral one-component systems, *Phys. Rev.* **94**(3):511–525(1954).
18. Y. Sone, Y. Waniguchi, and K. Aoki, One-way flow of a rarefied gas induced in a channel with a periodic temperature distribution, *Phys. Fluids* **8**(8):2227–2235 (1996).